Compact grating displacement measurement system with a 3 × 3 coupler

Chunhua Wei (魏春华), Shuhua Yan (颜树华)*, Cunbao Lin (林存宝), Zhiguang Du (杜志广), and Guochao Wang (王国超)

College of Mechatronic Engineering and Automation, National University of Defense Technology, Changsha 410073, China

**Corresponding author: yanshuhua996@163.com*

Received December 31, 2014; accepted March 16, 2015; posted online April 8, 2015

We present a compact displacement measurement system possessing the capability of nanometer-scale precision. On basis of integrating single grating with 3 × 3 coupler for phase shift in interference signal, the present scheme features advantages of simple structure, convenient alignment, and insensitivity to air turbulence. Linear comparisons between our system and HP5530 show a residual error less than 81 nm during step motions along a 10 mm round-trip, and a discrepancy less than 15 nm in the case of 200 μm movement. We also demonstrate a measurement stability test in a duration of 300 s, which shows the proposed scheme potentially performs better than HP5530 in terms of long-term stability.

OCIS codes: 050.1950, 060.2430, 060.2920.
doi: 10.3788/COL201513.051301.

Displacement measurement by optical interferometry has been an essential tool for nano-scale demand applications in industry and scientific research[1]. Up to date, although conventional laser interferometers working on heterodyne or homodyne principle are extensively used to measure the displacement with sub-nanometer resolution, the cost of that measurement system is still high, and the measurement accuracy depends on not only the stability of the laser wavelength, but also the compensation of air refractive index sensitive to the environment is tough to be precisely determined[2,3]. As another technology competent to realize displacement measurement with nanometers precision, grating interferometry provides measurement benchmark with a real object, and thus has a relatively low requirement for environmental conditions[4]. Resulting from the merits of low cost, simple configuration, and easy instrumentation, displacement measurement by grating interferometry attracts more and more attention in fields of biopharmaceuticals, ultra-precision machining, materials science, and so on.

Classical grating displacement measurement systems, such as the dual-grating measurement system, work on principles of Moiré fringe in a long range but with low resolution[5,6]. Recently, various types of grating interferometers have been developed to measure linear displacement or multi-degree-of-freedom (DOF) position with nanometer resolution, such as single-metric grating measurement system[7,8], Littrow-type grating interferometers[9,10], heterodyne grating interferometers[11,12], and DOF linear encoders[13]. Although most of these systems have their own merits and specific applications, they are usually built by relatively complicated optical setup, leading to difficulty in alignment. In this work, we focus on developing a compact and transportable grating interferometer for linear displacement measurement, which innovatively integrates the grating interferometry with a 3 × 3 coupler to construct a compact displacement measurement system. In this scheme, the optical path is minimized and DC noise of interference signals is suppressed, so the anti-jamming ability, measurement stability, and insensitivity to ambient change are largely enhanced, making it capable for precision measurement and potential for low-budget instrumentation.

The schematic configuration of the whole system is shown in Fig. 1. The single-wavelength laser beam emitted from the He–Ne laser is coupled into a single-mode fiber for possibility of distant delivery. The coupled beam from the other end of the single-mode fiber is collimated with a collimator, and then perpendicularly illuminates the surface of the reflection-type grating. After grating diffraction, the diffracted beams of the positive first order and negative first order reflect in the same diffraction angle. To acquire an interference signal, the symmetric diffracted beams of plus or minus first orders (denoted with P, Q) are coupled into the 3 × 3 coupler, and then optical interference signals with phase shifts are generated from the three outputs of coupler and detected by photo-detectors (PDs).

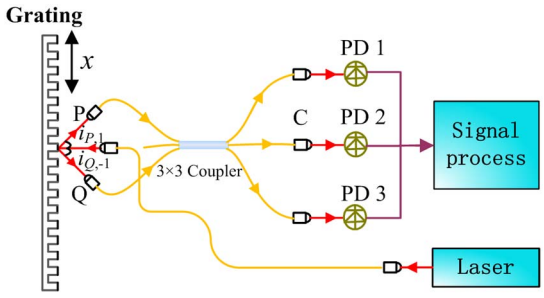

Fig. 1. Schematic diagram of the system configuration. C, collimator.

 © 2015 Chinese Optics Letters

Finally, these PD signals with interference fringe information are sent into a signal processing module for displacement calculation and display. Compared with other grating interferometers, the proposed scheme combines the metric grating with a 3×3 coupler to construct a low-cost optical interferometric measurement system which generates phase-shifted interference signals more succinctly. Besides, the optical system is easier and more flexible to be arranged in a compact and transportable module, which facilitates alignment and construction for short noncommon optical path exposed to air.

Suppose that $i_{P,1}$ and $i_{Q,-1}$ shown in Fig. 1 are the diffraction angles of the two beams P and Q, respectively; ν_0 is the frequency of the input laser beam; and d is the grating pitch. When the grating moves in direction x at a speed of V, the Doppler-shift related frequencies of two diffracted beams $(P,1)$ and $(Q,-1)$, $\nu_{P,1}$ and $\nu_{Q,-1}$, can be expressed as

$$\begin{cases} \nu_{P,1} = \nu_0 \cdot \frac{c}{c - V \sin i_{P,1}} \\ \nu_{Q,-1} = \nu_0 \cdot \frac{c}{c - V \sin i_{Q,-1}} \end{cases}. \tag{1}$$

After interference of two beams, the composite Doppler shift is equal to $\nu_{P,1} - \nu_{Q,-1}$. Allowing for the conditions that $i = i_{P,1} = -i_{Q,-1}$, $c \gg V$ and the grating diffraction equation $d \sin i = \lambda$, the composite Doppler shift can be deduced as

$$\Delta\nu = \nu_{P,1} - \nu_{Q,-1} \approx \frac{2V}{d}. \tag{2}$$

The detected fringe variation N during time T is an integral of Doppler shift

$$N = \int_0^T \Delta\nu \mathrm{d}t = \frac{2}{d}\int_0^T V \mathrm{d}t = \frac{2}{d}S, \tag{3}$$

where S is the displacement of the grating within time T. Thus, the targeted displacement is expressed as

$$S = N \cdot \frac{d}{2}. \tag{4}$$

Equation (4) indicates that the phase change is estimated to be 2π, when the grating moves by half of a grating pitch. In our system, we use a holographic grating[14] of 1200 grooves/mm. Hence, the interference signal repeats at every 416.7 nm of the grating movement.

In signal processing, interference signals from the 3×3 coupler with fixed phase shifts are vital for the accurate phase demodulation. With perfect design of a 3×3 coupler, including no power loss, no polarization state change, and equal split ratio, phase difference between two arbitrary outputs of the 3×3 coupler is 120° theoretically[15]. However, in practice, the actual condition of power loss, the split ratio and the polarization state in 3×3 coupler could not be perfect, so the phase shifts are not a constant of 120°, but contaminated by a phase deviation comprising a quasi-constant phase offset determined by split ratio and phase fluctuation related to polarization variation. Such phase deviation is possible to be evaluated by using the scattering matrix theory of fiber couplers. In our case, that deviation is theoretically estimated to be less than 6°, which is in good accordance with observation of actual interference signals. Instead of using specific disposal on fiber, such as polarization maintaining or tuning the split ratio, we implement phase compensation algorithm to accurately calculate phase change in fringe despite of these drifted phase deviations between interference signals[16]. The three interference signals output from 3×3 coupler can be written as

$$\begin{cases} a = A_1 \cos\theta \\ b = A_2 \cos(\theta + 120° + \Delta\varphi_2) \\ c = A_3 \cos(\theta + 240° + \Delta\varphi_3) \end{cases}, \tag{5}$$

where θ is the phase value to be measured; A_1, A_2, and A_3 are the respective amplitude values of three outputs; a, b, and c are real-time voltage of interference signals; $\Delta\varphi_2$ and $\Delta\varphi_3$ are the uncertain phase deviations. From Eq. (5), θ can be ultimately deduced as

$$\theta = a \tan\left\{\frac{a[A_2 \cos(120° + \Delta\varphi_2) - A_3 \cos(240° + \Delta\varphi_3)] - (b - c)A_1}{a[A_2 \sin(120° + \Delta\varphi_2) - A_3 \sin(240° + \Delta\varphi_3)]}\right\}. \tag{6}$$

In phase demodulation algorithm, values of A_1, A_2, A_3, a, b, and c are initially required, and then $\Delta\varphi_2$, $\Delta\varphi_3$, and θ can be obtained sequentially. We have also done 150 groups of simulation to test that demodulation algorithm. The standard deviation of the simulation result deviated from true value is 1.25°; in this context albeit phase deviations and amplitude errors were added to interference signals in the simulation, which corresponded to a displacement precision of about 1.45 nm.

On basis of phase demodulation algorithm, a signal processing module with high-speed analog-to-digital (A/D) converter and digital signal processor (DSP) was developed, which can realize fast and precise phase measurement. Figure 2 gives a schematic graph of the entire signal processing module. The three interference signals from the PDs are amplified at first, and then the amplified signals are sampled from analog signal to digital signal via high-speed A/D converter. Next, with sampling time

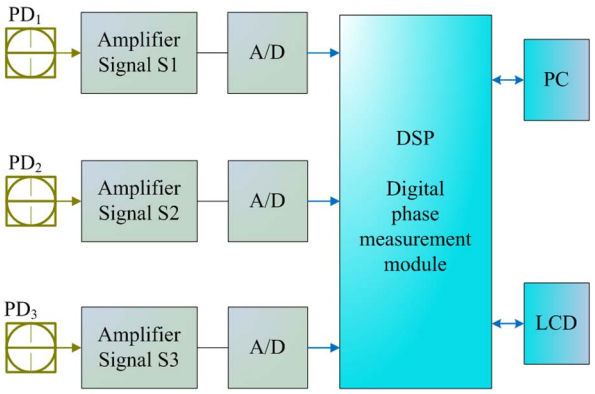

Fig. 2. Schematic diagram of signal processing module.

synchronization, the three sampled signals are transmitted to the DSP-based digital phase demodulation module to obtain accurate displacement. Finally, the displacement result can be transmitted to PC by data bus for data storage, and also can be displayed on a DSP-supported liquid-crystal display (LCD).

Figure 3 is a diagram for the prototype of our displacement measurement system. To evaluate the performance of the present system, we install a conventional laser interferometer (HP5530) on the same translational moving stage. All optical components are fixed on an anti-vibration stage except for HP5530 laser head fastened on a separate accessorial holder, which enhances reliability and stability of the comparative measurement.

Before the installation of the grating sample, manufactured with a length of 15 mm and a designed wavelength of 632.8 nm, a white light interferometer (Zygo New View 700) is used to test the grating's surface structure. The resolution (0.293 μm) of the interferometer is not high enough, so the 3D structure obtained is a little bit rough, shown in Fig. 4(a). The grating pitch is estimated using scanning electron microscopy (SEM), as shown in Fig. 4(b). By measuring the total length of a small random section covering 20 grating pitches, we average the grating pitch as approximately 831 nm, while it is predesigned to be 833 nm in principle, which shows acceptable manufacturing quality for grating. Manufacturing precision of grating is crucial for measurement accuracy as grating pitch is the basic measurement scale in this context[17]. Although the single grating pitch is impossible to be made equal and accurate due to inevitable random errors in manufacturing, such errors could be averaged and reduced by multiple pitches together.

The three interference signals with phase shifts can be observed directly by an oscilloscope (Tektronix DPO2024). Figure 5 shows the analog waveforms of three interference signals after amplifier. With the phase measurement function of DPO2024, the actual phase shifts of signals are measured to be 125.5° and 237.3° (−122.7° shown in Fig. 5), which correspond to phase deviations of 5.5° and −2.7° in good accordance with the previous phase estimation. Besides, the quality of signals after photoelectric conversion and amplification is identified quite high as shown from Fig. 5.

A stabilized He–Ne laser with a wavelength of 632.8 nm is used as the laser source in our system, matching with the grating design. On the large anti-vibration base stage, a motor platform is fastened to give common translational movement for grating and target mirror of HP5530. The movement is driven by an electronic-control motor platform KSA150-12-X and MC600-2B, which possesses a closed-loop resolution of 1 μm and a repeatability of 3 μm. Then comparative experiments are performed between our system and HP5530 laser interferometer.

To test the measurement performance of our system, first, a long-range linear comparison is performed. As the measurement range of our system is determined by the effective diffraction length of the grating as 15 mm, and the middle part (10 mm length) of the grating is chosen along with a step motion of 1 mm. A forward and backward movement of 10 mm range is sequentially performed,

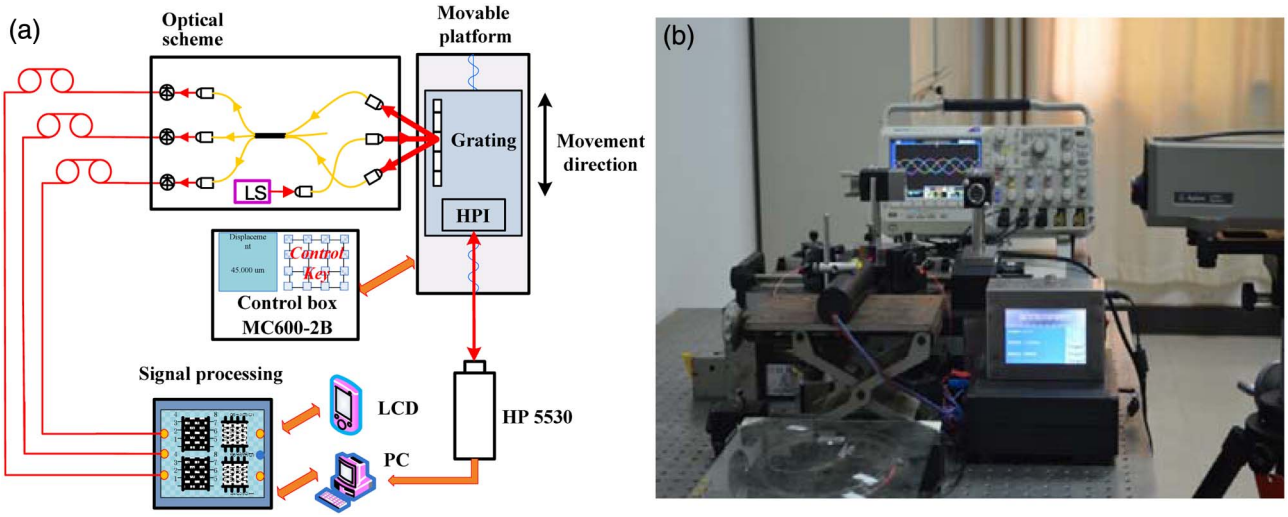

Fig. 3. Measurement system; (a) schematic diagram of the measurement system; (b) picture of the prototype of the measurement system. HPI, Hewlett Packard interferometer; LS, laser source; PC, personal computer.

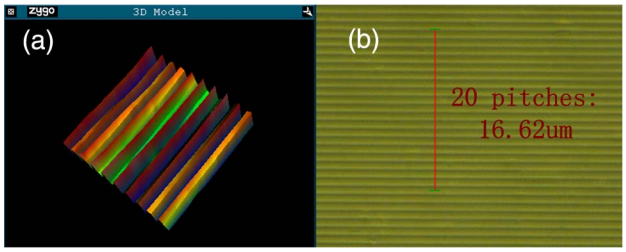

Fig. 4. Grating images; (a) by Zygo New View 700; (b) by SEM.

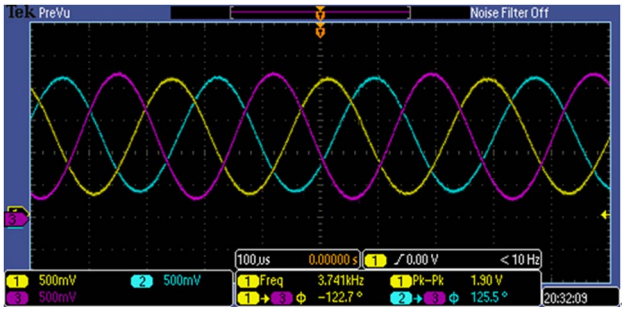

Fig. 5. Output of three interference signals.

and the measurement results are shown in Fig. 6, where the reference displacements in the x-axis come from the reading of the HP5530 and measurement results are recorded in 1 min for averaging after each step motion. Figure 6(a) directly shows the original differences in linear displacement between HP5530 and our system. As the displacement increases, it seems the difference also linearly increases, and the maximum is 559 nm at the location of 10 mm during the forward movement. There may be a cluster of factors accounting for the differences, but the main error results from the cosine error between the grating center axis and optical path of laser interferometer, so linear fitting is implemented for data processing. Residual errors are obtained by the subtraction between measurement results of grating system and fitted results. The fitted data and residual errors for forward movement and backward movement are shown in Figs. 6(b) and 6(c), respectively. The maximum residual error (absolute value) is no more than 81 nm during the round-trip movement. The fitted slope with a slight change is estimated from the tiny tilt of the platform moving axis between the forward movement and backward movement, which explains that there is about 86 nm offset when the platform returns to the initial position referenced to HP5530.

Relative to long-range comparison, we performed a short-range linear comparison as well. Because the closed-loop resolution of the electronic-control motor platform only reaches 1 µm corresponding to one driving pulse, each time we choose 25 step impulses to feed the amount of step motion, which are estimated to be from 25 to 200 µm. Figure 7 gives the comparison results of every step motion: the maximum of residual errors is less than 15 nm, while the peak-to-valley (PV) value is 23 nm, which confirms that our system is potential for comparative performance with laser interferometer in short-range measurement.

When the measurement stability of our system is tested, we turn off the electronic-control motor platform MC600-2B for removal of motor vibration. We initialize the measurement of the HP5530 and our system, and continuously monitor the displacement variation. Due to usage of the low internal memory DSP in the present system, the measurement update rate could not be high, so we set it at 1 s for assurance. Figure 8 shows the system stability measurement results of two measurement systems for 5 min. In Fig. 8(a), displacements of our method maintain quite well as time elapses, albeit there are some local drift around the initial value. Relatively, displacements of HP5530 have a small drift in a short time window, but accumulative offset arises as time elapses, which is estimated from refractive index change in the dead path. The results of our measurement have some initial drift, which is estimated to come

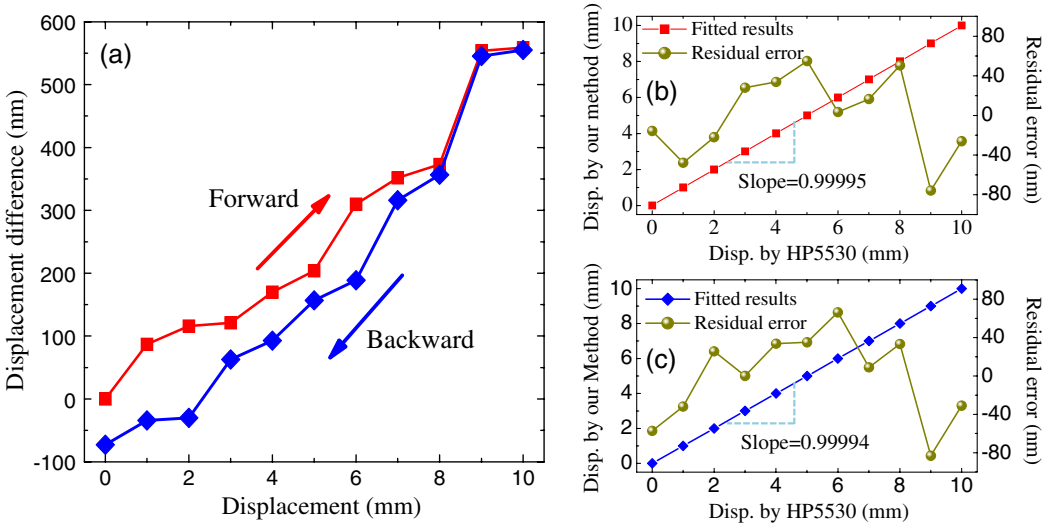

Fig. 6. Comparison measurement result of the 10 mm round-trip; (a) original displacement difference; (b) linear fitting and residual error for the forward movement; (c) linear fitting and residual error for the backward movement. Disp, displacement.

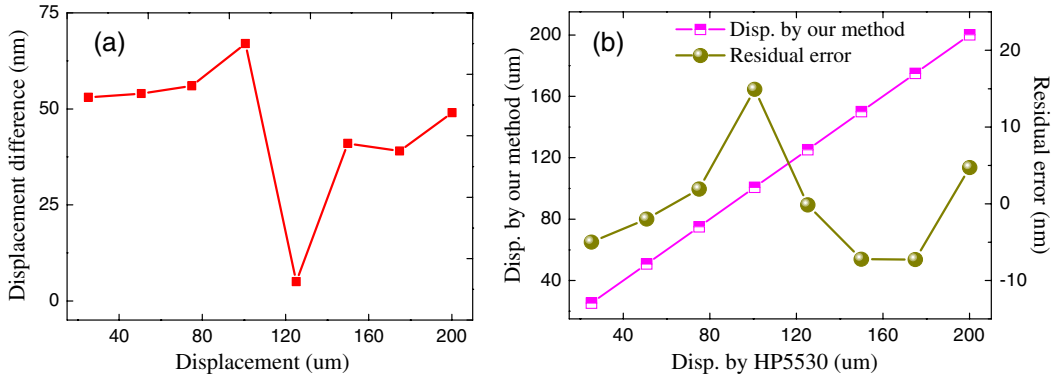

Fig. 7. Comparison measurement result of 200 μm movement; (a) original displacement difference; (b) linear fitting and residual error for the movement.

from intensity variation of the interference signals. Because a certain spatial gap still exists between the grating scale and the collimator for receiving light, when we press the reset button on LCD to initialize the measuring system, it would cause some air flow and a slight vibration close to our optical configuration. Displacement calculated by algorithm fluctuates at the beginning, and gradually becomes stable. Nevertheless, it is obvious that the center of displacement results seems unvaried. Besides, as a display resolution of 1 nm in our system, the displacement seems to maintain as a constant value during a short time such as 100–150 s. Figure 8(b) gives the Allan deviation analysis of the measurement data. The analysis indicates that, in a short time, the stability of HP5530 is better than that of our method, but in the long-term case, our method potentially shows better stability than HP5530.

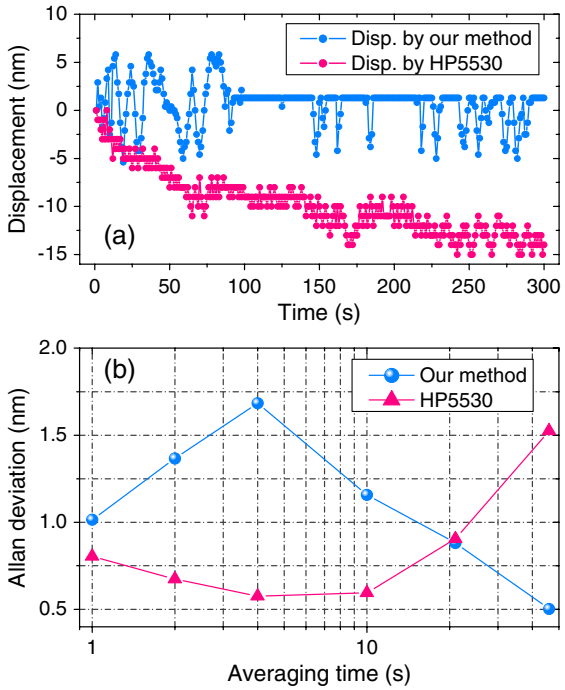

Fig. 8. Stability test results; (a) the system stability measurement results for our system and HP5530 for 300 s; (b) Allan deviation analysis of the measurement data.

In conclusion, we propose a displacement measurement scheme based on 3×3 coupler and single grating, and construct a measurement system with the advantages of high measurement precision, simple optical path, compact structure, and insensitivity to ambient change. Linear comparison experiments and stability test prove the competent performance of our system, which is promising as a low-budget choice in the fields of micro/nanofabrication, microelectronics engineering, biomedicine, and so on. For the next step, we also plan some further research on extending the measurement range, promoting data processing update rate, compact design for practical application, and studying systematic measurement error.

This work was supported by the National Natural Science Foundation of China under Grant No. 51275523.

References

1. J. Lazar, M. Holá, O. Číp, M. Čížek, J. Hrabina, and Z. Buchta, Opt. Express **20**, 27830 (2012).
2. N. Bobroff, Meas. Sci. Technol. **4**, 907 (1993).
3. S. Xu, L. Chassagne, S. Topcu, L. Chen, J. Sun, and T. Yan, Chin. Opt. Lett. **11**, 061201 (2013).
4. A. Teimel, Precis. Eng. **14**, 147 (1992).
5. H. Lu, J. Cao, S. Su, and G. Tang, Proc. SPIE **4077**, 40 (2000).
6. "Heidenhain exposed linear encoders," Online: http://www.heidenhain.com.
7. X. C. Chu, H. B. Lü, and S. H. Zhao, Meas. Sci. Technol. **19**, 017001 (2008).
8. F. Cheng and K. C. Fan, Appl. Opt. **50**, 4550 (2011).
9. C. C. Wu, C. C. Hsu, J. Y. Lee, Y. Z. Chen, and J. S. Yang, Opt. Commun. **297**, 89 (2013).
10. C. F. Kao, S. H. Lu, H. M. Shen, and K. C. Fan, J. Appl. Phys. **47**, 1833 (2008).
11. J. Y. Lee and M. P. Lu, Opt. Commun. **284**, 857 (2011).
12. G. Wang, S. Yan, and W. Zhou, Opt. Eng. **51**, 081512 (2012).
13. A. Kimura, W. Gao, and L. Zeng, Meas. Sci. Technol. **21**, 054005 (2010).
14. B. Deka and P. P. Sahu, Appl. Opt. **50**, E193 (2011).
15. S. T. Shih, M. H. Chen, and W. W. Lin, IEE Proc.-Optoelectron. **144**, 377 (1997).
16. C. Wei, S. Yan, C. Lin, G. Wang, and P. Zou, J. Optoelectron. Laser. **25**, 704 (2014).
17. X. Jiang, H. Huang, X. Wang, and L. Huang, Chin. Opt. Lett. **7**, 407 (2009).